

**Investigating the maximum resolution of  $\mu$ XRF core scanners: a 1800 year storminess reconstruction from the Outer Hebrides**

Lisa C Orme

University of Exeter, UK

Liam Reinhardt

University of Exeter, UK

Richard T Jones

University of Exeter, UK

Dan Charman

University of Exeter, UK

Ian Croudace

University of Southampton, UK

Alastair Dawson

University of Aberdeen, UK

Michael Ellis

British Geological Survey, UK

Andrew Barkwith

British Geological Survey, UK

**Corresponding Author:**

Liam Reinhardt, Department of Geography, Centre for Life and Environmental Science, University of Exeter, Cornwall Campus, Treliever Road, Penryn, Cornwall, UK. TR10 9FE. Email: [Liam.Reinhardt@exeter.ac.uk](mailto:Liam.Reinhardt@exeter.ac.uk). Phone: 01326 371868

**Abstract**

Micro X-ray fluorescence ( $\mu$ XRF) core scanning is capable of measuring the elemental composition of lake sediment at sub-millimetre resolution, but bioturbation and physical mixing may degrade environmental signals at such fine scales. The aim of this research is to determine the maximum possible resolution at which meaningful environmental signals may be reconstructed from lake sediments using this method. Sediment from a coastal lake in the Outer Hebrides, Scotland, has been analysed using calibrated element measurements, to reconstruct storminess since 200 A.D. We find that a Ca/K ratio in lake core sediments reflects the presence of fine calcium carbonate shell fragments, a constituent of sand in the catchment that is washed and blown into the lake. Variations in this ratio are significantly correlated with instrumental records of precipitation and low pressures, suggesting it is a proxy

for storminess. Furthermore, identification of a c.60 year cycle supports a climatic influence on Ca/K, as this cycle is frequently identified in reconstructions of the North Atlantic Oscillation and North Atlantic sea-surface temperature. Comparison with weather records at different resolutions and spectral analysis indicate that  $\mu$ XRF data from Loch Hosta can be interpreted at sub-decadal resolutions (equivalent to core depth intervals of 3-5 mm in this location). Therefore we suggest that sub-centimetre sampling using  $\mu$ XRF core scanning could be beneficial in producing environmental reconstructions in many lake settings where sediments are not varved.

**Key words**

XRF core scanner, lake sediment, Late Holocene, storminess, North Atlantic Oscillation

## **Introduction**

Rapid, very high (sub-millimetre) resolution element analysis on sediment cores can be achieved non-destructively using Micro X-ray Fluorescence ( $\mu$ XRF) core scanners (Croudace et al., 2006). This method, while still considered novel, has been used to create reconstructions of past environmental change from lake sediment deposits (e.g. Giguet-Covex et al., 2011; Metcalfe et al., 2010; Moreno et al., 2008; Yancheva et al., 2007). Bioturbation (mixing) of benthic sediment occurs through the movements of flora and fauna: this has been found to occur over depths of 3-20 cm (Krantzberg, 1985; Lee, 1970) but the effects are unevenly distributed within lakes (White and Miller, 2008). Sediment disturbance can also occur from re-deposition by currents and sediment slumping (Hilton et al., 1986). Therefore, traditional methods of sediment analysis (typically  $\geq 1$  cm resolution) may not preserve the signature of environmental changes and at the sub-millimetre resolution of  $\mu$ XRF analysis the influence of disturbance is likely to be enhanced. Some studies using  $\mu$ XRF have dealt with this issue by using varved and laminated lake sediment sections where the influence of bioturbation can be shown to be minimal, enabling annually resolved climate records to be produced (e.g. Giguet-Covex et al., 2011; Metcalfe et al., 2010). However, when

dealing with homogenous lake sediment the effect of bioturbation on proxy measurements is less clear.

To investigate the maximum sampling interval of  $\mu$ XRF analysis that produces reliable results (and the age resolution that this corresponds to at this location) analysis was carried out on two cores from a lake on North Uist, an island in the Outer Hebrides, western Scotland. This location was selected as an environment likely to be sensitive to variations in the North Atlantic Oscillation (NAO), which is a measure of the pressure difference between the Azores High and the Icelandic Low (Hurrell, 1995; Van Loon and Rogers, 1978). The NAO influences cyclonic formation and the location of the storm track in Europe, so is a strong influence on the frequency and intensity of storms (or storminess) in this region (Hurrell, 1995; Serreze et al., 1997). In this paper, calibrated  $\mu$ XRF data, specifically  $\text{Ln}(\text{Ca}/\text{K})$ , are used to produce a Late Holocene palaeo-storminess reconstruction. Calcium was investigated as there are abundant sources of calcium-rich sand in close proximity to the lake, while potassium was selected as a suitable denominator due to higher concentrations in the catchment soil than the beach sand. Therefore, the premise is that higher  $\text{Ln}(\text{Ca}/\text{K})$  values occur when Ca-rich sand is deposited into the lake by storms, either directly or by deposition onto the catchment and subsequent inwashing.

The climatic influence on the elemental changes, as well as the maximum resolution producing reliable palaeoenvironmental reconstructions, is

determined using a number of methods. The initial interpretation is based on elemental analysis of catchment sediment sources, sedimentological analysis of the cores and comparison with instrumental climate data. To determine the maximum resolution, the reconstruction is correlated with instrumental climate records at a range of age resolutions to identify which produces the strongest correlations. Assessment of cyclicity in the record is then used to support the climate influence on the lake sediment and the optimum resolution. Reconstructions of the NAO have identified cycles of c.20, 40, 60 and 70-90 years (Appenzeler et al., 1998; Cook et al., 1998; Glueck and Stockton, 2001; Higuchi et al., 1999; Luterbacher et al., 1999; Wanner et al., 2001) and in a 5200 year reconstruction cycles of 170 and 350 years were identified (Olsen et al., 2012). Similar cycles of 40-100 years are characteristic of the Atlantic Multidecadal Oscillation, which is a measure of Atlantic Ocean temperatures (Enfield et al., 2001; Gray et al., 2004; Kerr, 2000; Knudsen et al., 2011), and may be present in reconstructions, given that it is thought coupled atmosphere-ocean interactions control climate in the North Atlantic region (Higuchi et al., 1999; Olsen et al., 2012; Yang and Myers, 2007). Therefore, detection of these cycles within the data is a way of assessing the influence of the climate on the lake sediment and the highest frequency cycle identified will provide an indication of the maximum reliable age resolution and sampling interval of the reconstructions.

## **Study area**

Loch Hosta (57°37'30"N 7°29'8"W) is a low lying lake (measuring 0.27 km<sup>2</sup>, up to 11m deep, at an altitude of 10 m) on the west coast of the Outer Hebridean island of North Uist (Figure 1). The climate of the Outer Hebrides (based on Stornoway station measurements, 1981-2010 A.D.) is mild, wet and windy, with an average annual precipitation of 1250 mm, temperatures between 6 - 11 °C and on average winds around 11 knots (equivalent to 5.7 m s<sup>-1</sup>; Met Office, 2014a). Historical records indicate that the NAO has a strong control on storms in this region, with a positive correlation between the NAO and wind speed, gale days, precipitation and cyclone occurrence since 1950 A.D. (Andrade et al., 2008; Marques et al., 2008; Pirazzoli et al., 2010). Severe storms periodically influence the Outer Hebrides, for example, hurricane force winds in January 2005 caused sand dune retreat, flooding and coastal erosion and records indicate two other storms of even greater magnitude since 1980 A.D. (Dawson et al., 2007). The exposed situation of the lake means it is likely to be highly sensitive to the high winds and precipitation brought by severe storms, and these are likely to cause sediment erosion, transport and deposition into the lake.

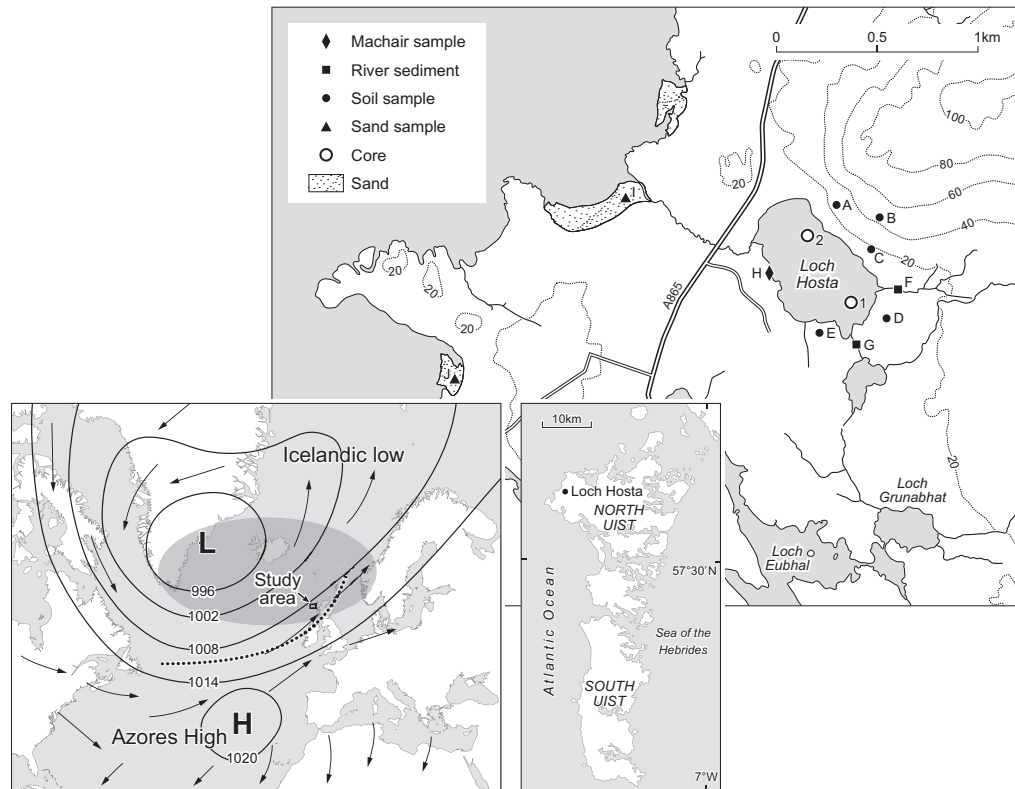


Figure 1: Map of Loch Hosta, situated at 57°37'30"N 7°29'8"W on North Uist (Outer Hebrides). Labels 1 and 2 represent the coring locations of the sediment cores Hosta 1 and Hosta 2 respectively. Labels A-J represent sampling locations of soil and sand from the catchment. *Inset left*: Schematic diagram of the location of the Outer Hebrides, and the North Atlantic Oscillation pressure centres (Azores High and Iceland Low). The shaded area is the region with increased cyclone numbers when there is a positive NAO index (>1) (based on the results of Andrade *et al.*, 2008). *Inset right*: Location of Loch Hosta in the Outer Hebrides.

Loch Hosta was selected as it is surrounded by sources of calcium rich sand, which may be entrained either by aeolian or fluvial processes during storms. Sources of calcium carbonate-rich shell sand for aeolian transport are the nearby beaches, and the machair; a rare, sand-based, grassland ecosystem adjacent to Loch Hosta (Angus, 1997). The coastal location of the lake may also mean that sea-spray is blown into the lake during storms, although the concentration of Ca in sea water is small (0.04 %) (Kirk and Moberg, 1933). Ca deposition is also likely to occur by overland flow from the hill bounding the north eastern side of Loch Hosta and from two tributary streams that enter the lake at the southern end and drain a small, hilly catchment to the east of the lake. The catchment bedrock is Lewisian grey gneiss, which is typically formed of quartz, plagioclase feldspar, biotite and hornblende, with Ca concentrations of 3-7% (Angus, 1997; Smith and Fettes, 1979; Weaver and Tarney, 1981). Sediment originating from such bedrock contains low Ca; as we show later catchment soil does contain Ca (<10%) most likely originating from both the bedrock as well as from wind-blown carbonate sand. Calcium can precipitate in some lakes due to biological processes (Dittrich and Obst, 2004; Leng et al., 2001; Stabel, 1986), however these are most often where calcium saturation has occurred, which is unlikely in a grey gneiss bedrock catchment. Therefore the dominant source of Ca in Loch Hosta sediments are wind-driven beach deposits that either blow directly into the lake or first onto adjacent hill slopes,

which thereafter wash down into the lake during rainfall (or perhaps more slowly by soil creep).

Changes to the catchment in the past by either human or natural processes may have influenced sediment input to the lake. At present the land around Loch Hosta is predominantly grazing pasture for cattle, but includes a few houses. The adjacent hill slope is known to once have had a settlement called Baleloch is thought to have been established in 1666 A.D. until depopulation around 1815 A.D. (Canmore, 2014; Moisley, 1961). The distance between the coastline (sand sources) and the lake may also have varied due to relative sea level changes: a reconstruction from the Outer Hebridean island of Harris shows <0.5 m of sea level rise since c. 1 A.D. (Jordan et al., 2010), however, even with stable sea level, coastal changes can occur depending on the offshore topography and sand supply (Cattaneo and Steel, 2003; Hansom, 2001). These anthropogenic and environmental changes are necessary considerations in the interpretation of variations in the lake sedimentology.

## **Methods**

### *Catchment sampling*

To determine the element composition of allochthonous sediment entering Loch Hosta nine sand and soil samples were collected from the adjacent machair, beaches, rivers and fields, at the locations shown on Figure 1. These samples were treated using hydrogen peroxide to remove organic

material and sieved to separate the <500 µm fraction, as this fraction is easily transported by aeolian and fluvial processes (Kok et al., 2012). The samples were subject to XRF analysis at X-ray Mineral Services (Colwyn Bay, Wales), where they were dried at 105°C, crushed into a fine powder, blended with lithium metaborate and fused at 1080°C into a glass "bead". XRF analysis was performed using a Spectro X-Lab Energy Dispersive (polarised) XRF Spectrometer, following standard procedures (Stephens and Calder, 2004) and calibrated using international standards.

#### *Lake sediment core extraction*

Coring of Loch Hosta was undertaken in September 2011 using a short (1 m) Mackereth corer (Mackereth, 1969) at two locations shown in Figure 1, called Hosta 1 and Hosta 2. To minimise the influence of bioturbation, cores were taken from depths >4 m (Hosta 1 at 4.8 m and Hosta 2 at 5.3 m), as in most lakes faunal activities are concentrated between 2 and 4 m in the photic zone (White and Miller, 2008). Cores were extracted within plastic tubes and transported vertically. In the laboratory, excess water was removed and the cores were extruded from their tubes, split into two longitudinally and put into semi-circular plastic tubes, which were wrapped with plastic film. The cores were stored in a cold store.

#### *µXRF element analysis and calibration*

High resolution  $\mu$ XRF and X-radiographic measurements (of sediment density) were taken by an ITRAX XRF core scanner (Croudace et al., 2006) at the National Oceanography Centre, Southampton. During scanning an X-ray (transmitted through a capillary waveguide to ensure high intensity) irradiated the sediment of the split core surfaces and the secondary or fluorescent X-rays generated from excited elements in the sample were detected by an electrically cooled energy dispersive X-ray detector (SDD). An X-ray energy spectrum was acquired, stored and analysed for each measurement point. The machine used a Mo-tube, voltage of 30 kV, current of 50 mA, exposure time of 20 seconds and a step size of 200  $\mu$ m. The results were initially normalised using the sum of incoherent and coherent counts (inc + coh) measured by the ITRAX core scan to account for Compton and Raleigh scattering (as done by Kylander et al., 2011). Following this the covariance between elements was assessed using a 10 cm moving window.

A methodological limitation of  $\mu$ XRF analysis is that it produces *relative* element variations based on X-ray counts or count-rates, and therefore the measurements can be influenced by a range of inter-element effects. Significant down-core changes in organic, water or carbonate content can impact elemental responses (e.g. the 'dilution effect' and 'matrix effect'; see Löwemark et al., 2010). However researchers can confirm the quantitative validity of their data by independently analysing a sub-set of samples using a traditional, destructive method (e.g. WD-XRF, ICP-OES). Therefore we have calibrated the

$\mu$ XRF data using the log-ratio calibration equation method of Weltje and Tjallingii (2008), which calibrates the  $\mu$ XRF using XRF measurements and expresses the results as natural log-ratios.

To calibrate, sixteen XRF sub-samples (each 1 cm thick) were taken from points along the cores selected to represent the extremes of the  $\mu$ XRF data (as recommended by Weltje and Tjallingii, 2008). These sub-samples were dried to 100 °C and 0.5 g was taken and mixed with 5 g lithium tetraborate (Fluxana, GmBh). The mixtures were fused at 1100 °C in Pt-Au crucibles and cast into Pt-Au dishes to produce a set of glass disks (Croudace & Williams Thorpe, 1988), which were analysed using a Philips Magix-Pro wavelength dispersive XRF spectrometer (also at Southampton National Oceanography Centre). The  $\ln(\text{Ca}/\text{K})$  ratio of the calibration (XRF) samples and the  $\mu$ XRF data (averaged over the equivalent 1 cm depth) were then calibrated (see detailed method in Weltje and Tjallingii, 2008) and the relationship between these expressed as a Log Ratio Calibration Equation (LRCE):

$$\ln\left(\frac{W_{Ca}}{W_K}\right) = \alpha \ln\left(\frac{I_{Ca}}{I_K}\right) + \beta$$

where  $I_{Ca}$  and  $I_K$  are the  $\mu$ XRF intensity values and  $\ln(W_{Ca}/W_K)$  is the calibrated  $\mu$ XRF results. The success of the calibration was assessed using the Goodness of Fit ( $R^2$ ) equation (see Weltje and Tjallingii, 2008).

### *Chronology*

The success of any climate reconstruction rests on the quality of the age model used to reconstruct the temporal framework for the data set. Age-depth models are often based on methods such as radiocarbon dating, with potentially large errors, and/or models that rely on interpolation between dated horizons (Telford et al., 2004). With high resolution reconstructions these chronological errors are large in comparison to the timescales of interest (Moberg et al., 2005), so these may influence  $\mu$ XRF reconstructions. Therefore, to support the investigation of the optimum age resolution, we consider a selection of potential chronologies that lie within the age errors, to assess the influence of age-depth model selection on the results.

$^{210}\text{Pb}$  was used to date the upper sediment of each core. Samples taken every 2-3 cm were dried, ground gently, sealed in plastic tubes and left for 21 days to achieve radioactive equilibrium. Analysis was made by gamma assay (measuring activity of  $^{210}\text{Pb}$ ,  $^{226}\text{Ra}$  and  $^{137}\text{Cs}$ ) with the Constant Rate of Supply (CRS) model (Appleby, 2001; Appleby and Oldfield, 1978; Goldberg, 1963). To ascertain dating accuracy the  $^{210}\text{Pb}$  ages were compared against increased levels of  $^{137}\text{Cs}$  in the cores, caused by nuclear weapons tests between 1953 and 1963, and the 1986 Chernobyl nuclear disaster (Pennington et al., 1973; Ritchie et al., 1973).

One sample near the base of each core was AMS radiocarbon dated using bulk sediment, as above-ground plant macrofossils were not present.

These were dated at Queens University Belfast's <sup>14</sup>CHRONO centre. The radiocarbon dates were calibrated and the age-depth models created using OxCal version 4.2.3, using the IntCal13 calibration curve and Bayesian analysis (Bronk Ramsey 2009; Bronk Ramsey and Lee, 2013; Reimer et al., 2009, 2013). The median of the 2-sigma age range was used to estimate the age for individual samples down the cores. These are referred to as 'OxCal models' hereafter.

As the age-depth models in this study were poorly constrained, we explored how subtle variations in the models influence the results. This was done by selecting age-depth curves that produced the best correlations between the measured sand content of both cores within the age errors, as a way of tuning the two records to common environmental signals. To do this 3000 age-depth power-law curves were randomly fitted to each core, with each fit lying within the 2-sigma dating error bars. We chose power-law fits on the assumption that the deposition rate is steady and increasing sediment compaction is expected with depth (e.g. Christensen, 1982). The best 100 age-depth fits from each core were then used to calculate the mid-point age of each 1 cm section of measured down-core sand mass. The variability in sand deposition through time was then correlated between the two cores for all 100 pairs of possible age-depth fits. All 10 000 possible combinations were explored and those with the best correlations were selected. Thus the selected age-depth fits a) meet the physical constraints of deposition and compaction, b) fit within

assigned age error bars and c) tune the age-depth data to common environmental signals experienced at both core locations. It is important to note that we calibrated the age-depth fits using the sand-fraction weight results to avoid circularity, i.e. sand weight is used to calibrate the best age-depth fits and these fits are then applied to independently measured  $\mu$ XRF  $\text{Ln}(\text{Ca}/\text{K})$  ratio data. Hereafter the group of age-depth models with high correlations are referred to as 'grouped models'. The pair of models that correlated most strongly are termed 'main models' and are used in figures and results unless otherwise stated. Dated  $\mu$ XRF results are then independently tested against instrumental climate data over the past c.130 years to ascertain how well the common environmental lake-core signals correlate with historical climate variability.

#### *Proxy data analysis*

Loss-on-ignition was carried out to identify the relative changes in organic and inorganic content using 5 cm<sup>3</sup> of wet sediment taken every 1 cm along both cores. Samples were dried at 105°C overnight, ignited in a furnace at 550°C for 4 hours and weighed before and after each stage (Dean, 1974; Heiri et al., 2001). Following this the inorganic material was sieved to identify the sand-sized sediment. Prior to sieving, the inorganic material was disaggregated by being put in 0.4% sodium hexametaphosphate (Bamber, 1982), left for 24 hours and then put in an ultrasonic bath for two minutes.

Sieving was carried out to separate the 120-180  $\mu\text{m}$  and  $>180 \mu\text{m}$  sediment fractions; the lower boundary for sieving was selected to remove the potential influence of distal tephra deposits, which are in the range of 10-100  $\mu\text{m}$  in size (Hall and Pilcher, 2002).

Further sediment was sampled at the 1 cm resolution for the Carbon:Nitrogen (C:N) analysis, to identify the sources of organic matter from allochthonous, terrestrial sources ( $>20$  C:N) or autochthonous sources such as algae (4-10 C:N), which can be related to catchment runoff and lake productivity (Meyers, 1994; Silliman et al., 1996). Sediment was freeze-dried, ground and weighed to 4-12 mg using a Sartorius Supermicro Balance machine. Analysis of the C:N content was done in a Flash 2000 Organic Element Analyzer.

Following the above analyses, the carbonate content was measured. Given the abundant calcium carbonate shell sources surrounding the lake, carbonate measurements were considered likely to resemble the combined silt and sand concentrations. Sediment was exhausted at some depths, particularly where sampling for the XRF calibration and  $^{210}\text{Pb}$  dating had been carried out, so measurements of this proxy are discontinuous. Analysis was done by repeating the loss-on-ignition method outlined above and then following it with ignition of the samples at  $1050^\circ\text{C}$  for two hours to remove the carbonate, before reweighing (Dean, 1974; Heiri et al., 2001).

To compare measurements, both the high resolution Ln(Ca/K) results and low resolution proxy datasets had to be re-sampled at the same resolution. To do this the 90<sup>th</sup> percentile age interval of the 1 cm resolution age-depth model was calculated. Both the proxy and Ln(Ca/K) results were re-sampled to this resolution, by interpolating, smoothing and down- (or up-) sampling. Spearman's correlations were then carried out, with the 95% significance of the result determined using the associated  $p$  value.

#### *Instrumental data comparison*

Instrumental weather records from Stornoway in the Outer Hebrides were correlated with the Ln(Ca/K)  $\mu$ XRF results, using Spearman's rank correlation method (with the 95% significance determined using the  $p$  value). This was carried out using the main, grouped and OxCal age-depth models. The climate records correlated were of winter (NDJF), summer (JJA) and annual temperature and precipitation (1873-2012 A.D.; Met Office, 2014b), the lowest 10<sup>th</sup> percentile of atmospheric pressure from Stornoway (1867-2010 A.D.) calculated using pressure records from the Edinburgh Met Office archives and a winter (NDJF) NAO index (1823-2012 A.D.; Climate Research Unit, 2004; Jones et al., 1997). To test the optimum resolution of the  $\mu$ XRF results, the correlations were made at a range of age resolutions (between 1 and 20 years). Re-sampling was carried out by smoothing then down sampling each dataset to

the chosen age resolution. Finally, the  $\text{Ln}(\text{Ca}/\text{K})$  was correlated against a millennial length winter NAO reconstruction (1049-1995 A.D.; Trouet et al., 2009) to investigate the long-term influence of this circulation pattern on the climate of the Outer Hebrides.

### *Spectral analysis*

Cycles were analysed using the Lomb-Scargle spectral analysis method for unevenly spaced data (Lomb, 1976; Press and Rybicki, 1989; Scargle, 1982; calculated using Shoelson, 2001). Spectral analysis was carried out to show the highest resolution achievable using  $\mu\text{XRF}$  data: noise from the core scanner and sediment is unlikely to exhibit cyclicity, so therefore the highest-frequency, significant cycle present provides an indication of the maximum resolution of the preserved climate reconstruction. Cycles can only be identified when they are twice the sampling resolution, also called the Nyquist frequency (Grenander, 1959), so 20 year cycles would suggest that the climate signal at the 10 year resolution had been preserved. The sensitivity to age-depth model selection was assessed by analysing the spectral frequency using the main, grouped and OxCal age-depth models.

Finally, cross-spectral analysis (Chatfield, 2004) between the  $\text{Ln}(\text{Ca}/\text{K})$  record and the Trouet et al. (2009) NAO reconstruction was carried out to identify shared spectral frequencies. This method was used to indicate the periodicities at which the NAO was driving storminess. For this the significance

level was calculated as follows: for 5000 iterations the Ln(Ca/K) and NAO datasets were randomised and cross-spectral analysis carried out, in order to capture the range of spectral magnitudes at each frequency that can occur randomly, i.e. significant results are those that arise <5% of the time after random mixing of the data. The 95<sup>th</sup> percentile of these results provided the 95% significance level.

## **Results**

### *Catchment Elements*

The XRF results from the catchment (Figure 2) have been grouped and averaged into two sets: sand samples from the beach and machair, which are sources of sediment for aeolian transport, and soil samples from the hill slopes and tributaries, which will reflect sediment that may wash in. The sand samples were composed primarily of Ca (29-43%) and Si (14-35%), with small concentrations of K (0.2-0.8%), while the soil from the catchment and rivers had high Si content (55-67%), as well as Fe (4-8%), Al (13-15%), Ca (4-9%) and K (1.2-1.6%). Although the catchment soil was not high in K, the Ln(Ca/K) ratio of the soil was on average 1.4, compared to 4.3 for the sand samples, therefore

increases in the lake sediment  $\text{Ln}(\text{Ca}/\text{K})$  are expected to reflect greater beach sand input.

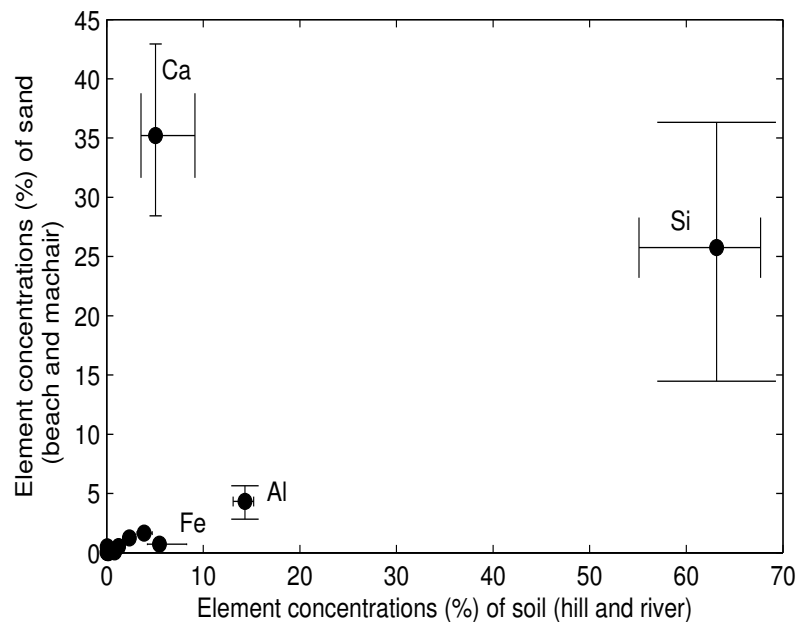


Figure 2: Composition of the major elements present in sand and soil samples from the Loch Hosta catchment. The average element measurements of the soil samples (based on the mean of 6 soil and river sediment samples: shown on Figure 1) are shown along the x-axis and the average of the sand samples (based on the mean of 3 samples from the machair and beaches) are shown along the y-axis. The range of element concentrations for both sand and soil samples are shown by the vertical and horizontal error bars respectively.

### *Core composition*

The two cores were retrieved with the sediment-water interface intact. In length Hosta 1 was 54 cm and Hosta 2 was 56 cm. The two cores were stratigraphically homogeneous, black to very dark brown in colour and composed of organic lake mud with silt/sand.

The  $\mu$ XRF core scan measured high counts of 12 elements including some considered as potentially useful for this research: Ca, K, Ti, Fe, Mn, Rb and Br (shown in Figure 3). The total number of counts (kcps) and mean squared error (MSE) measurements indicate good detection levels over most sections of core, with occasional MSE peaks influencing single measurements (Figure 3). The X-radiographic images, reflecting sediment density, show distinct horizons of dense sediment that appear to correspond to peaks in Ca, K, Ti, Fe and Mn (Figure 3). To assess the relationships between Ca and the other elements the covariance was calculated (Figure 3). The covariance in both cores is strongest between Ca-K and Ca-Ti (with maximum values of c.0.6) and lowest between Ca-Br. In Hosta 1 there is particularly low covariance below 30 cm depth, while Hosta 2 varies throughout the core.

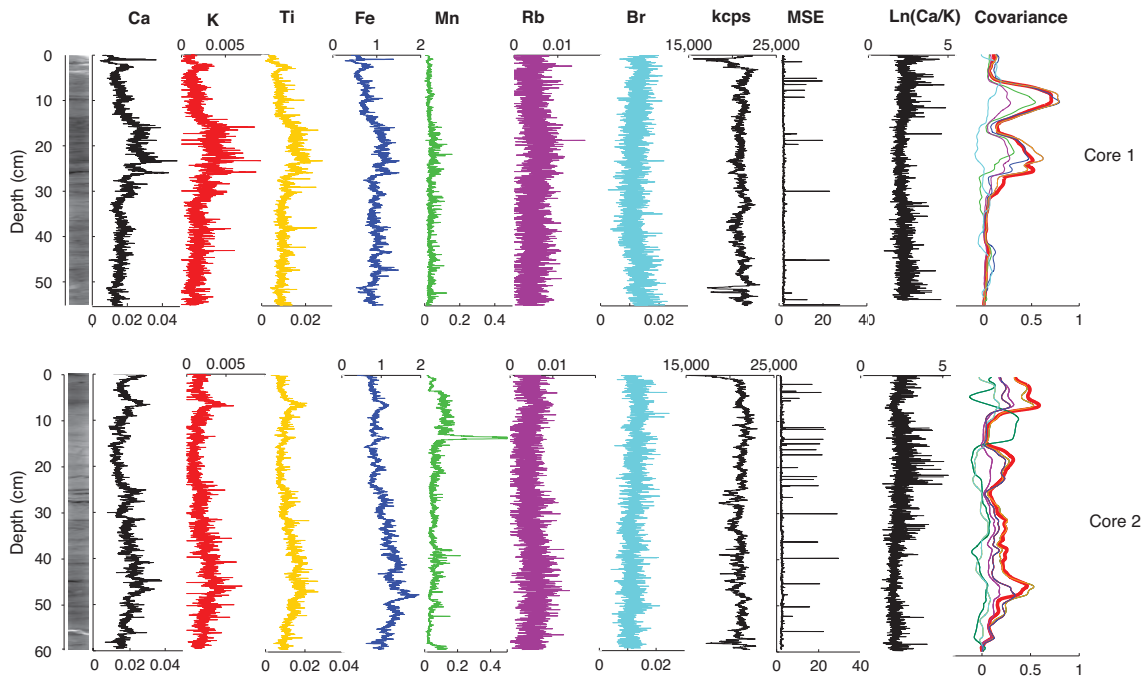


Figure 3: Raw X-radiograph and  $\mu$ XRF element results. From left: the radiograph image (dense sediment indicated by darker shades), the Ca, K, Ti, Fe, Mn, Rb and Br results normalised with the sum of incoherent and coherent counts (inc + coh), the total number of element counts (kcps), the Mean Standard Error (MSE), the calibrated  $\text{Ln}(\text{Ca}/\text{K})$  results and the results of down core changes in the covariance between Ca and other elements. The kcps and MSE reflect the sediment matrix being scanned (Kylander et al., 2012). The covariance analysis was carried out using a moving window spanning 10 cm. The elements used in the covariance plot are shown by the corresponding colours of the element plots.

Conservative elements such as Al and Rb are often used for normalisation (e.g. Guyard et al., 2007; Löwemark et al., 2010), however Al was poorly detected by the ITRAX scanner and Rb was not measured by the XRF analyses used for calibration, so could not be used. The calibration was initially carried out using a range of denominators that were elements present in the catchment soil (Fe, Ti, K), and the calibration using K showed the highest Goodness of Fit statistic ( $R^2 = 0.86$ ). Although K can be influenced by dissolution and weathering within lake sediments following deposition (Löwemark et al., 2010) we do not believe that this has greatly affected the results here. There exists a strong correlation between the  $\mu$ XRF Rb/(inc+coh) and K/(inc+coh) results of  $R=0.82$  and  $R=0.92$  in Hosta 1 and 2 respectively, showing the K results are highly similar to those of a conservative element from the same source. The  $\text{Ln}(\text{Ca}/\text{K})$  calibration resulted in LRCE parameters of  $\alpha = 0.309$  and  $\beta = 0.794$ .

### *Chronology*

$^{210}\text{Pb}$  dating of the cores offers little constraint for the age-depth modelling, due to the large analytical errors (Table 1) and in Hosta 1  $^{210}\text{Pb}$  activity was only detected in the upper 2 cm of sediment. Nonetheless we were able to produce a wide range of plausible fits that allowed us to explore the sensitivity of the final results to the age-depth fits used: models with the strongest significant correlation between the sand fraction results are shown in

Figure 4. The best of these (the main models) resulted in a correlation of  $R = 0.59$  between the sand content of the two cores. Selection of the top-500 correlations between pairs of age-depth models resulted in many duplicates, so that in fact the grouped age models consisted of only 26 and 9 unique models for Hosta 1 and 2 respectively. The main, grouped and OxCal models are used to assess the sensitivity of the results to the model selection. The resulting age-depth models of Hosta 1 and 2 span the period since 260 and 820 A.D. respectively, although this is determined by age-depth model extrapolation from the lowest dated points to the bottom of the cores. Although these age-depth models are not well constrained, the homogenous stratigraphy supports that the depositional environment has remained relatively stable, so it is assumed that there are no hiatuses.

Core and sample Depth (cm)	Dating Method (Laboratory code)	$\delta^{13}\text{C}$ (‰)	Radiocarbon Age ( $^{14}\text{C}$ yr BP $\pm 1 \sigma$ )	Age (A.D.) ( $2\sigma$ error)	Calibrated Age (A.D.) ( $2\sigma$ range)
Hosta 1: 0-1	$^{210}\text{Pb}$	--	--	2001 $\pm$ 90	--
Hosta 1: 1-2	$^{210}\text{Pb}$	--	--	1964 $\pm$ 434	--
Hosta 1: 43-44	Radiocarbon (UBA-20599)	-32.3	1379 $\pm$ 30	--	652 (607-681)
Hosta 2: 0-1	$^{210}\text{Pb}$	--	--	2006 $\pm$ 33	--
Hosta 2: 1-2	$^{210}\text{Pb}$	--	--	1995 $\pm$ 37.8	--
Hosta 2: 3-4	$^{210}\text{Pb}$	--	--	1968 $\pm$ 60.2	--
Hosta 2: 5-6	$^{210}\text{Pb}$	--	--	1939 $\pm$ 129.2	--
Hosta 2: 47-48	Radiocarbon (UBA-20600)	-30.6	1071 $\pm$ 33	--	975 (895-1021)

Table 1: Results of  $^{210}\text{Pb}$  and radiocarbon dating of samples from Hosta 1 and Hosta 2. Note: the  $^{210}\text{Pb}$  date at 1-2 cm in Hosta 1 was not used to create the age-depth model due to the large errors associated with this date.

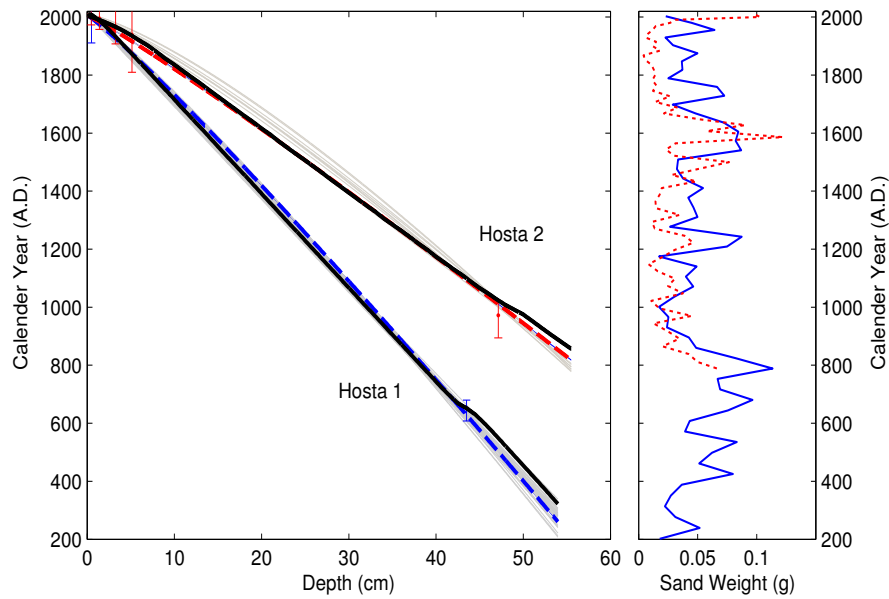


Figure 4: *Left* Age-depth models for Hosta 1 and 2. Dashed lines are the selected age model for Hosta 1 (blue) and Hosta 2 (red), while thick, continuous lines show the OxCal age models. Thin grey lines are the multiple age-fit curves calculated (see methods section). Two sigma error bars are shown for horizons dated using  $^{210}\text{Pb}$  and radiocarbon methods. There are three dated horizons for Hosta 1 and five for Hosta 2 (detailed in Table 1). *Right*: The selected age models are those with the strongest correlation between the two cores sand weight results, shown for Hosta 1 (continuous blue line) and Hosta 2 (dashed red line)

The  $\text{Ln}(\text{Ca}/\text{K})$  results (Figure 5 E and F) show an increase in  $\text{Ln}(\text{Ca}/\text{K})$  prior to c.1000 A.D. and after 1600 A.D., with low values between 1000-1400 A.D.. After 1900 A.D. the  $\text{Ln}(\text{Ca}/\text{K})$  results decrease until 1950 A.D. when they again increase. The cores show highly similar trends, supporting the contention that the results are capturing common environmental changes in the lake. A difference between the cores is that Hosta 2 has increasing values of  $\text{Ln}(\text{Ca}/\text{K})$  between 1400 A.D. and 1900 A.D. while in Hosta 1 the values only increase after 1600 A.D.

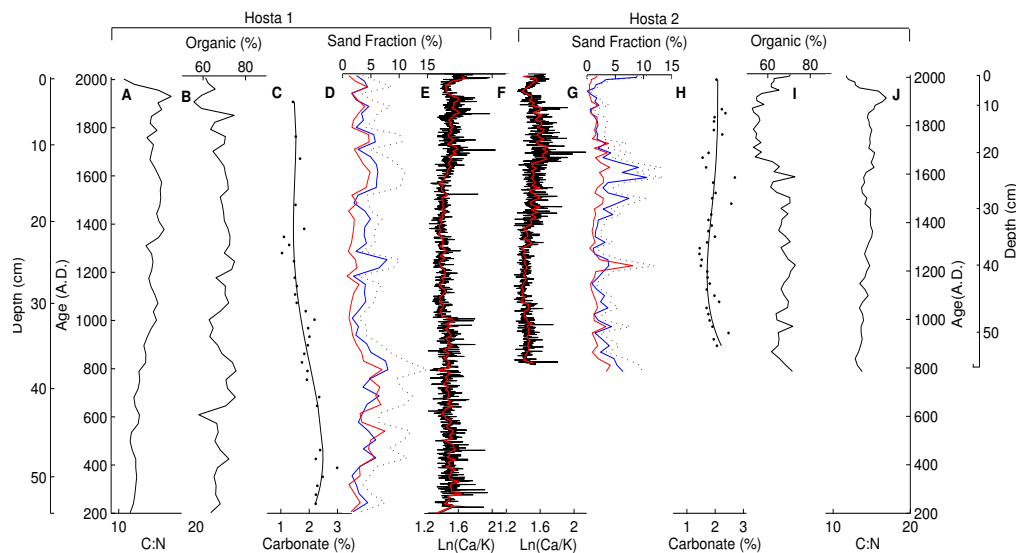


Figure 5: Hosta 1 and Hosta 2 sediment analysis results and  $\mu\text{XRF}$   $\text{Ln}(\text{Ca}/\text{K})$  results. The  $\mu\text{XRF}$   $\text{Ln}(\text{Ca}/\text{K})$  results (E and F) are smoothed and down-sampled to 1-year resolution for Hosta 1 and 2. Other proxies are the C:N analysis (A and J), organic percentage found using loss-on-ignition (B and I), irregularly sampled carbonate percentage estimated using loss-on-ignition, including

polynomial trend lines (C and H) and the sand fraction weights (D and G) in 5 cm<sup>3</sup> wet volume of sediment (red thin line = 120-180 µm fraction, blue thick line = >180 µm fraction, dashed line = 120-180 and >180 µm fractions combined).

### *Proxy Analyses*

To investigate if allochthonous sediment inputs to the lake were an important influence on Ca content, the Ln(Ca/K) and C:N ratio results were compared, as the C:N ratio can vary with changes in terrestrial carbon deposition and therefore runoff. The results are uncertain as the C:N values of 10-18 are between the levels considered as representing algal (4-10) and terrestrial carbon (>20) (Figure 5 A and J; Meyers, 1994). Furthermore, the correlation between Ln(Ca/K) and C:N is significantly negative at Hosta 1 (R = -0.43) and insignificantly positive at Hosta 2 (R = 0.29). Positive correlations would be expected if runoff was the dominant factor influencing both the C:N and Ln(Ca/K) content of the cores, however it is possible that the correlations may have been influenced by the different analytical resolutions used in each method.

We next sought to quantify the Ln(Ca/K) ratios down core by comparing with measured sand content. Hosta 1 had a fairly consistent sand content of 5-10% of the dry mass, while Hosta 2 had a sand content of <5% but with a peak to 10% between 1400-1800 A.D.. To compare the high resolution Ln(Ca/K)

results with the low resolution sand fraction results, each record was re-sampled to the same resolution, which for Hosta 1 was 40 years and Hosta 2 was 30 years. The combined 120-180 and >180  $\mu\text{m}$  sand percentages had an insignificant correlation of  $R = 0.26$  with Hosta 1  $\text{Ln}(\text{Ca}/\text{K})$  and a significant  $R = 0.32$  with Hosta 2  $\text{Ln}(\text{Ca}/\text{K})$ . An explanation for the low correlations may be that the sediment smaller than 120  $\mu\text{m}$  was not measured by the sieving method, and may have more of an influence on the  $\mu\text{XRF}$  measurements than the coarser fractions.

This suggestion is visually supported by the available carbonate measurements (Figure 5, C and H), which are likely to reflect the total  $\text{CaCO}_3$  shell fraction of the sediment. These vary between 1-3% of the dried weight, and show similar changes to the  $\text{Ln}(\text{Ca}/\text{K})$  results. As the  $\mu\text{XRF}$  core scanning method only measures Ca in the surface of the sediment, to a maximum depth of 1 mm (Löwemark et al., 2010; Weltje and Tjallingii, 2008), it is suggested that coarse sand distributed through the sediment was less likely to be present on the core surface than the fine sand. The potential effects of Ca sediment grain size on detection by the  $\mu\text{XRF}$  core scanners is detailed in the Supplementary Information. This indicates that in theory there is an exponential increase in the number of particles in the sediment as grain size decreases, so small grains may be more distributed through the sediment and therefore more likely to be detected by the core scanners.

### *Instrumental data comparison*

We next sought to confirm that elemental  $\mu$ XRF data may be used as a climate proxy by comparing it with instrumental climate data. The first step in this task was to determine the sample resolution that we should work at by correlating with instrumental precipitation data at different resolutions (between 1 and 20 years). The analysis was carried out using all the age-depth models being investigated.

The Hosta 1 results (Figures 6A and 6B) demonstrate that both the OxCal and main models produce significant correlations between  $\text{Ln}(\text{Ca}/\text{K})$  and precipitation at almost all resolutions. Notably, not all of the grouped models produce  $\text{Ln}(\text{Ca}/\text{K})$  results that correlate with the precipitation data, which implies that the interpretation of proxy data is highly dependent on obtaining a reliable age-depth model. The second core (Hosta 2) does not correlate significantly with precipitation when using any of the age-depth models, indicating that precipitation driven changes in runoff are not influencing this coring location. The changes in correlation (using Hosta 1) can be used to infer the optimum resolution of the data in this location, where the influence of bioturbation and other (noisy) mixing processes are minimised. The correlations between the selected Hosta 1  $\text{Ln}(\text{Ca}/\text{K})$  record and annual precipitation are significant at all

resolutions less than 10 years, but are at times insignificant at resolutions greater than 10, therefore  $R = 0.62$  at 10 years is taken as the maximum correlation achievable, which is equivalent to 3-5 mm sediment depth (Figure 6D). Other versions of the age-depth model, including the OxCal model, correlate more strongly with precipitation, however each of these reach the maximum correlation at approximately the 10-year resolution.

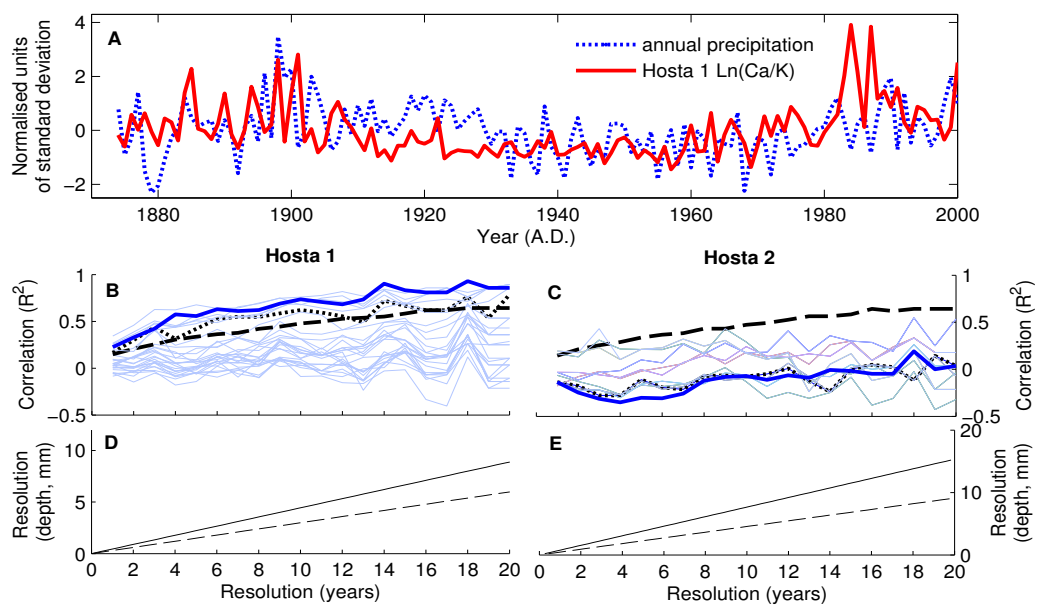


Figure 6: Comparison between Ln(Ca/K) and precipitation data. A: normalised Stornoway annual precipitation plotted against the Hosta 1 normalised Ln(Ca/K) from 1870-2000 A.D.. B and C: correlation between annual precipitation and the Hosta 1 Ln(Ca/K) (B) and Hosta 2 Ln(Ca/K) (C) at resolutions between 1 and 20 years, using the selected age model (dotted black line), the OxCal age model (continuous blue line) and the alternative age models shown in Figure 2

(narrow, light blue lines). The dashed line indicates the 95% significance level. D and E: conversion between the average depth and resolution for the instrumental period (black line) and full core (dashed line) for Hosta 1 (D) and Hosta 2 (E).

Having determined the optimum resolution we smoothed and downsampled the Ln(Ca/K) records of both cores, as well as all of the climate indices, to the 10 year resolution and calculated the correlations between these. Hosta 1 correlated significantly with annual precipitation ( $R = 0.76$ ;  $n = 13$ ) and low pressures ( $R = -0.63$ ,  $n = 14$ ), which supports that low pressure storms bring greater amounts of sand into the lake, however the correlation with the winter NAO ( $R = 0.22$ ;  $n = 18$ ) was insignificant. Hosta 2 did not correlate significantly with annual precipitation, low pressures or the winter NAO, however the correlation with annual temperature was negative and significant ( $R = -0.68$ ,  $n = 13$ ). The correlations between the Ln(Ca/K) results and the NAO reconstruction of Trouet et al. (2009) at the 10-year resolution showed significant negative correlations in both Hosta 1 ( $R = -0.49$ ,  $n = 95$ ) and Hosta 2 ( $R = -0.62$ ,  $n = 95$ ).

### *Spectral analysis*

The variability of the Hosta 1 Ln(Ca/K) has been assessed through Lomb-Scargle spectral analysis (as this core had the strongest storminess signal) to identify the optimum reliable resolution of the  $\mu$ XRF-based climate

reconstruction. Again, we used the main, grouped and OxCal models in our analysis, as a means of assessing the sensitivity of the results to age-depth model selection. The analysis showed many centennial scale cycles (Figure 7), including those of c.860, 250-200, 153-139 and 105-95 years, which are significant in all or most of the age-depth models. Shorter cycles of 77-87 and 50-58 years are also present in many of the age-depth models. The shortest cycle of 16-20 years is only significant in the results of one age-depth model, although many show an insignificant peak at this frequency. The comparison with instrumental climate data indicated that the optimum resolution of Hosta 1 was 10 years, and the identification of the 16-20 year cycle, which has a Nyquist frequency between 8 and 10 years, supports that this is the case. Finally cross-spectral suggests analysis of the main Hosta 1 Ln(Ca/K) record with the Trouet et al. (2009) NAO reconstruction showed shared cycles of 256 and 60 years, which implies an NAO influence on the Ln(Ca/K).

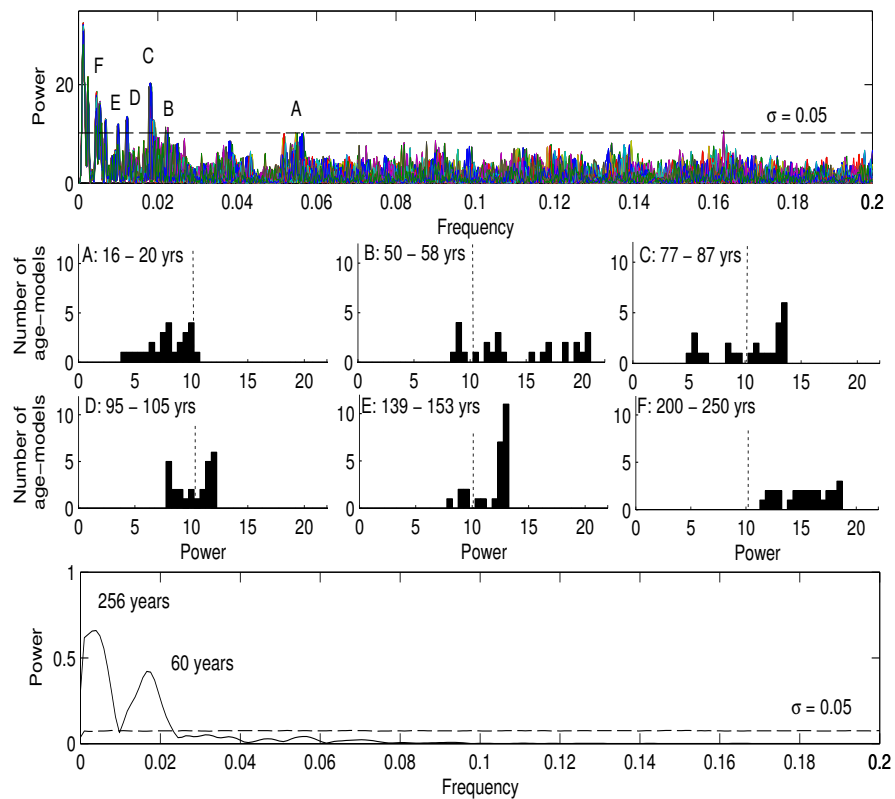


Figure 7: *Top*: The Lomb-Scargle spectral analysis of the Hosta 1 Ln(Ca/K) using the age models shown in Figure 1. The dashed, black line illustrates the  $\sigma=0.05$  significance level and labels A-F show the significant peaks, which correspond to histograms A-F. *Middle*: Histograms showing the powers of spectral peaks at specified frequencies produced from the different age-depth fits. Results to the right of the dotted line are statistically significant at the 95% confidence level. *Bottom*: cross-spectral analysis results between the Hosta 1 Ln(Ca/K) results and the Trouet et al. (2009) NAO reconstruction. The black line indicates the  $\sigma=0.05$  significance level.

## **Interpretation**

Before investigating the resolution of the climate signal preserved in the cores it is necessary to interpret the available results to explore the causes and pathways of sediment deposition to the lake. As the  $\text{Ln}(\text{Ca}/\text{K})$  of catchment sand was higher than that of soil samples, it is inferred that for high  $\text{Ln}(\text{Ca}/\text{K})$  values to occur in the lake sediment, beach sand must have been deposited, either directly into the lake through aeolian transport or blown onto the catchment and subsequently washed into the lake via tributaries or overland flow.

Hosta 1 was sampled from close to the tributaries (Figure 1), so it is likely to have been influenced by riverine plumes of sediment associated with high precipitation (Hilton et al., 1986). This interpretation is supported not only by the strong correlation of the Hosta 1  $\text{Ln}(\text{Ca}/\text{K})$  with precipitation, but also by the high covariance between the (uncalibrated) Ca and K, Fe and Ti results (Figure 3), which supports a deposition of minerogenic soil at this site. Furthermore, as sand sized particles do not saltate across water and are too large to have been blown in suspension across the lake (Kok et al., 2012), the presence of higher sand percentages in Hosta 1 than Hosta 2 further supports that a riverine plume deposits sediment at this site.

The correlation with precipitation records and the evidence of deposition from the riverine plume points to the  $\text{Ln}(\text{Ca}/\text{K})$  being a precipitation proxy.

Nevertheless the distribution of elements in the catchment (i.e. higher Ca/K ratios of the beach sand), and the correlation with the low pressure record (associated with both rain and wind) supports that the Hosta 1 record reflects aeolian sand deposition to the catchment from storms, which is then washed into the lake. The aeolian influence cannot be assessed further however due to a lack of long records of wind speed from this area. This interpretation means there may be a lag between large storms that transport sand to the catchment and deposition in the lake; however at the multi-annual resolutions of the records, we consider that it is unlikely to have resulted in a temporal offset.

A question that arises is whether general storminess changes or extreme events cause the sand deposition represented by the  $\ln(\text{Ca/K})$  and the measured sand content. As sand is present throughout the cores this may support that sand is delivered during storms that occur with multi-annual to decadal frequency (given the age resolutions of the records). This is further supported by the correlation with precipitation and low pressures during the instrumental period; as the instrumental records are annual or seasonal averages these reflect general patterns rather than individual extreme events. Nevertheless, as there is a non-linear relationship between sand transport and wind speed (Bagnold, 1941), it is likely that when rare and extreme storms occur, a large amount of sand may be deposited over the lake and catchment. It remains a challenge therefore to establish whether rare, extreme storms or multiple, small magnitude storms were responsible for the observed changes.

The results indicate that the sedimentation at Hosta 2 is quite different to Hosta 1. Hosta 2 is located further from the tributaries and there appears to be no influence from sediment plumes. This is indicated by low correlations between the Hosta 2  $\text{Ln}(\text{Ca}/\text{K})$  and the precipitation and low pressure records and a lower and more variable sand content, suggesting sedimentation is more sporadic (Figure 5). As the core was sampled from closer to sand sources along the north western edge of the lake, the deposition here is considered more likely to result from aeolian transport. This in some respects contradicts the visual similarity between the long-term  $\text{Ln}(\text{Ca}/\text{K})$  trends shown by the two cores; the reason may be that the changes seen in both cores were the result of large magnitude storminess changes influencing both coring sites, whereas the low magnitude variability of the instrumental period only influenced the Hosta 1 coring site closest to the tributaries, which can be considered a more sensitive reconstruction. Instead, Hosta 2 had a moderately strong, negative correlation with temperature, however the reason for this is unclear. Higher temperatures may cause drier sand in the catchment, and therefore enhanced sediment erosion and transport (e.g. Kok et al., 2012), but this would result in a positive correlation. Similarly, autochthonous sources of Ca produced by lake biology would also be expected to positively correlate with temperature (Leng et al., 2001).

## **Discussion**

### **Methodological assessment**

The primary aim of this research was to assess the maximum resolution at which reliable data is produced by  $\mu$ XRF scanning of lake sediment cores, given possible disturbance from bioturbation and basal lake currents, among other causes (Krantzberg, 1985; Lee, 1970). The presence of horizontal layers within the sediment, as shown by the radiograph images (Figure 3), provide an initial indication that bioturbation has not greatly mixed the sediment. We investigated this further by correlating the Hosta 1  $\text{Ln}(\text{Ca}/\text{K})$  with precipitation data at different resolutions and spectral analysis. In Hosta 1 the maximum correlation at 10 years, as well as the cycle of 20 years (which has a Nyquist frequency of 10 years), indicated the optimum reliable resolution was reached at  $\sim$ 10 years resolution (representing 3-5 mm). However, even at higher resolutions the correlations were significant, which suggests that sediment disturbance degraded rather than destroyed the climatic signal in the sediment (Lee, 1970; White and Miller, 2008). At this 10-year resolution results are the average of measurements from 3 mm sample thickness, across a 4 mm wide scanning cross-section and to X-ray penetration depths of 1 mm (Croudace et al., 2006). Therefore the averaging of the element measurements over both width and depth may reduce the influence of sediment mixing. Overall, the

evidence suggests that bioturbation in the deepest part of Loch Hosta has not removed an environmental signature. Therefore in lakes with similar levels of disturbance, as determined by factors including lake bathymetry and climate, the  $\mu$ XRF core scanning method is likely to enable sub-centimetre sampling.

When performing the spectral analysis and correlations with climate data, a range of potential age-models were analysed. The correlation with instrumental climate data showed that the results are sensitive to the chosen age-depth model, presumably because the size of the age errors (and therefore the potential range of ages for each sample) are large compared to the length and resolution of the instrumental data. On cores with better dating constraints this problem may be limited. The spectral analysis of the results indicated that detection of low-frequency cycles was less sensitive to the age-depth model selection; however the higher frequency cycles were much more sensitive, for example the 16-20 year cycle was only significant in one age-depth model. This could be because the errors in the dating were often larger than the cycles being detected, causing the age-depth models to distort the cycle. These results highlight an issue with  $\mu$ XRF core scanning analysis, as although the method allows high sub-millimetre resolution data to be produced (Croudace et al., 2006; Weltje and Tjallingi, 2008), the results are sensitive to age uncertainty.

Finally, our results indicated that  $\mu$ XRF elemental analysis may be most sensitive at detecting fine sediment changes (see Supplement 1), as coarser

sand fractions were found to not correlate strongly with the  $\text{Ln}(\text{Ca}/\text{K})$  measurements. Similarly a lake precipitation reconstruction from the Alps found low correlations between coarse sand and  $\mu\text{XRF}$  calcium results, which was suggested as being the result of the analyses being carried out on different sediment from the same depth and sediment deformation during coring (Giguet-Covex et al., 2011). However we suggest that the fine-scale  $\mu\text{XRF}$  measurements may be capturing changes in the amount of very fine Ca-rich silt rather than the sand. This is suggested as there was a similarity between the  $\text{Ln}(\text{Ca}/\text{K})$  and the carbonate measurements, which reflect grains of all sizes. Our calculations showed an exponential increase in the number of particles in the sediment as the grain size decreases, which supports that the finer sediments will be more dispersed within the sediment and therefore more likely to be detected by the  $\mu\text{XRF}$  core scan of the surface sediment. Alternatively, elements may be enriched in certain particle sizes as a result of their geological origin, for example K is often associated with clays (e.g. Cuven et al., 2010; Kylander et al., 2011), so this may also explain the low correlations between the sand fraction and  $\text{Ln}(\text{Ca}/\text{K})$  results.

### **Late Holocene climatic and environmental change**

The results indicate that the Little Ice Age (1400-1850 A.D.) was a period of enhanced storminess, as shown by the  $\text{Ln}(\text{Ca}/\text{K})$  results of both cores and the higher sand content in Hosta 2 at 1400-1800 A.D.. As Hosta 2 was from

close to the beaches and away from the tributaries, this may show that there were extreme aeolian events at this time. The  $\text{Ln}(\text{Ca}/\text{K})$  records correlated negatively with the Trouet et al. (2009) NAO reconstruction spanning the past millennium, which contrasts with the positive correlation between precipitation/storms and the NAO observed in the instrumental period (Andrade et al., 2008; Hurrell and Van Loon, 1997). This shows long-term discontinuity of the storm-NAO relationship; for example the Little Ice Age would be expected to have had calm and dry conditions in northwest Scotland given the reconstructed negative NAO (Trouet et al., 2009), however the results indicate that storminess was higher. Other research supports these findings, showing increased Little Ice Age storminess across Europe including the Outer Hebrides (Dawson et al., 2004; Gilbertson et al., 1999; Sorrel et al., 2012), which it has been hypothesised was caused by intensified storms resulting from a steeper latitudinal temperature gradient (Trouet et al., 2012). Our  $\text{Ln}(\text{Ca}/\text{K})$  records are therefore capturing the climate deterioration associated with the Little Ice Age.

Many of the cycles identified are similar to those identified in NAO reconstructions. The 16-20 year cycle is similar to a ~20 year cycle which has been identified in previous NAO reconstructions (Cook et al., 1998; Glueck and Stockton, 2001; Luterbacher et al., 1999; Olsen et al., 2012). The c.60 year cycle identified by the spectral and cross-spectral analyses are similar to a c.60 year cycle often identified in NAO reconstructions (Cook et al., 1998; Glueck and Stockton, 2001; Luterbacher et al., 1999; Olsen et al., 2012; Wanner et al.,

2001) as well as in the GISP2 sodium reconstruction of storminess spanning the last 1000 years (Fischer and Mieding, 2005). The cycles of 50-58 and 77-87 years also resemble cycles of the Atlantic Multidecadal Oscillation index of North Atlantic Ocean temperatures, which varies with periodicities of 60-80 years (Enfield et al., 2001; Gray et al., 2004; Higuchi et al., 1999; Kerr, 2000; Knudsen et al., 2011; Wanner et al., 2001). The results support an ocean-atmosphere climate link controlling storminess and precipitation patterns over multi-decadal timescales (Higuchi et al., 1999; Olsen et al., 2012; Yang and Myers, 2007).

The impact of human activities and sea level changes are necessary considerations as these may have influenced the results presented here. It is possible that human activities in the vicinity of the lake may have increased the amount of sediment deposited by increasing catchment erosion. The nearby small settlement of Baleloch (Canmore, 2014; Moisley, 1961), coincides with the period when the  $\text{Ln}(\text{Ca}/\text{K})$  is high in Hosta 1 and 2. Furthermore, changes through time of sediment availability could be caused by sea level changes, influencing the distance between the coastline and sand sources. Despite relative sea level in the Outer Hebrides having changed by  $<0.5$  m since c. 1 A.D. (Jordan et al., 2010), the offshore topography and variable sediment availability may have caused local transgressions (Cattaneo and Steel, 2003; Hansom, 2001). Despite these uncertainties, the above correlations with the long NAO reconstruction and the instrumental climate indices, as well as the

cycles present that reflect those associated with the NAO and AMO, support that the Loch Hosta Ln(Ca/K) reconstruction is capturing a climatic signal.

## **Conclusion**

Past changes in storminess in the Outer Hebrides since 200 A.D. have been reconstructed using high resolution  $\mu$ XRF core scanning elemental analysis. The Ln(Ca/K) ratio in a core sampled from close to tributaries correlated with instrumental records of precipitation and low-pressures, suggesting that storms deliver pulses of sediment onto the catchment and then into the lake.

By identifying high frequency cycles (of 16-20 years) and correlating the results with instrumental weather records it was shown that the optimum resolution at which reliable climate proxy results can be obtained in Loch Hosta was 10 years, or 0.3-0.5 cm. Therefore meaningful, sub-centimetre sampling resolutions can be attained using  $\mu$ XRF analysis. Proxies that offer annual resolution results, such as speleothem reconstructions or varved lake sediments, are not present in many regions; therefore the  $\mu$ XRF method provides a widely applicable alternative for high resolution terrestrial climate reconstructions. In addition, it was found that the correlation with instrumental

data, and the identification of high frequency cycles in particular, were highly sensitive to the age-depth model used; the standard OxCal age-depth model offered one of the most robust solutions, while low frequency cycles were identified using most of the tested age-depth models. This is thought to be due to the relatively large dating errors (and therefore the large range of possible ages for each sample depth) compared to the frequency of the short cycles and the high resolution of the instrumental data.

Our storminess reconstruction has distinct centennial-scale changes, including a period of higher storminess at c.1400-1900 A.D., which can be related to the Little Ice Age. The results support previous findings that the Little Ice Age had high storminess, despite a negative NAO phase and an associated southerly storm track, something which has been suggested as being due to higher storm intensities (Trouet et al., 2012). Spectral analysis, and cross-spectral analysis with a long NAO reconstruction (Trouet et al., 2009), supported a climatic influence from the NAO and ocean temperatures, particularly as 16-20 and 60-year cycles were identified. These results indicate that there is a strong climatic influence on Loch Hosta sediments resulting from regional storminess.

### **Acknowledgments**

The authors would like to thank Rose Ferraby, Fraser Sturt, Duncan Garrow, Rebecca Rennell and Kate MacDonald (of Uist Archaeology) for fieldwork

assistance and Angela Elliot, James Grapes, Sue Franklin, Neville England, Mark Grosvenor and Mandy Lee for laboratory assistance. Thanks to Helen Jones for creating the site map (Figure 1).

### **Funding**

This work was supported by the British Geological Survey (50% funding through the BUFI scheme; grant number 4060003820/S191) and the Royal Geographical Society with the New Research Worker Award.

### **Bibliography**

Andrade C, Trigo RM, Freitas MC et al. (2008) Comparing historic records of storm frequency and the North Atlantic Oscillation (NAO) chronology for the Azores region. *Holocene* 18: 745-754.

Angus S. (1997) *The Outer Hebrides/The Shaping of the Islands*. England: The White Horse Press.

Appenzeller C, Schwander J, Sommer S et al. (1998) The North Atlantic Oscillation and its imprint on precipitation and ice accumulation in Greenland. *Geophysical Research Letters* 25: 1939-1942.

Orme et al. (2015) *The Holocene*. DOI: 10.1177/0959683615596819

Appleby PG (2001) Chronostratigraphic techniques in recent sediments. In: Last WM, Smol JP (eds.) *Tracking environmental change using lake sediments*. The Netherlands: Kluwer Academic Publishers, pp. 171-203.

Appleby PG and Oldfield F (1978) The calculation of  $Pb^{210}$  dates assuming a constant rate of supply of unsupported  $Pb^{210}$  to the sediment. *CATENA* 5: 1-8.

Bagnold RA (1941) *The Physics of Blown Sand and Desert Dunes*. London: Methuen.

Bamber RN (1982) Sodium hexametaphosphate as an aid in benthic sample sorting. *Marine Environmental Research* 7: 251-255.

Bronk Ramsey C (2009) Bayesian analysis of radiocarbon dates. *Radiocarbon* 51: 337-360.

Bronk Ramsey C and Lee S (2013) Recent and planned developments of the program OxCal. *Radiocarbon* 55: 720-730.

Canmore (2014): North Uist, Loch Hosta, Baleloch. Available at:

<http://canmore.rcahms.gov.uk/en/site/10109/details/north+uist+loch+hosta+baleloch>

(Accessed 17/10/13).

Cattaneo A and Steel RJ (2003) Transgressive deposits: a review of their variability. *Earth-Science Reviews* 62: 187-228.

Chatfield C (2004) *The Analysis of Timeseries: An Introduction*. CRC Press, Florida.

Christensen ER (1982) A model for radionuclides in sediments influenced by mixing and compaction. *Journal of Geophysical Research: Oceans* 87: 566-572.

Climate Research Unit, University of East Anglia (2004): North Atlantic

Oscillation data. Available at: <http://www.cru.uea.ac.uk/cru/data/nao/> (Accessed 10/01/14)

Cook ER, D'Arrigo RD and Briffa KR (1998) A reconstruction of the North Atlantic Oscillation using tree-ring chronologies from North America and Europe. *The Holocene* 8: 9-17.

Croudace IW, Rindby A and Rothwell RG (2006) ITRAX: description and evaluation of a new multi-function X-ray core scanner. In Rothwell RG (ed.) *New techniques in sediment core analysis. Geological Society, London, Special Publications* 267: 51-63.

Croudace IW and Williams-Thorpe O (1988) A low dilution, wavelength-dispersive X-ray fluorescence procedure for the analysis of archaeological rock artefacts. *Archaeometry* 30: 227-236.

Cuven SP, Francus P and Lamoureux SF (2010) Estimation of grain size variability with micro X-ray fluorescence in laminated lacustrine sediments, Cape Bounty, Canadian High Arctic. *Journal of Paleolimnology* 44: 803-817.

Dawson A, Elliott L, Noone S et al. (2004) Historical storminess and climate 'see-saws' in North Atlantic region. *Marine Geology* 210: 247-259.

Dawson AG, Dawson S and Ritchie W (2007) Historical climatology and coastal change associated with the 'Great Storm' of January 2005, South Uist and

Benbecula, Scottish Outer Hebrides. *Scottish Geographical Journal* 123: 135-149.

Dean WE (1974) Determination of carbonate and organic matter in calcareous sediments and sedimentary rocks by loss on ignition; comparison with other methods. *Journal of Sedimentary Research* 44: 242-248.

Dittrich M and Obst M (2004) Are picoplankton responsible for calcite precipitation in lakes? *AMBIO: A Journal of the Human Environment* 33: 559-564.

Enfield DB, Mestas-Nuñez AM and Trimble PJ (2001) The Atlantic multidecadal oscillation and its relation to rainfall and river flows in the continental US. *Geophysical Research Letters* 28: 2077-2080.

Fischer H and Mieding B (2005) A 1,000-year ice core record of interannual to multidecadal variations in atmospheric circulation over the North Atlantic. *Climate Dynamics* 25: 65-74.

Giguet-Covex C, Arnaud F, Poulénard J, et al. (2011) Changes in erosion patterns during the Holocene in a currently treeless subalpine catchment inferred from lake sediment geochemistry (Lake Anterne, 2063 m a.s.l., NW French Alps): The role of climate and human activities. *The Holocene* 21: 651-665.

Gilbertson DD, Schwenninger J, Kemp R et al. (1999) Sand-drift and Soil Formation Along an Exposed North Atlantic Coastline: 14,000 Years of Diverse

Geomorphological, Climatic and Human Impacts. *Journal of Archaeological Science* 26: 439-469.

Glueck MF and Stockton CW (2001) Reconstruction of the North Atlantic Oscillation, 1429-1983. *International Journal of Climatology* 21: 1453-1465.

Goldberg E (1963) Geochronology with  $^{210}\text{Pb}$ . In: *Proceedings of a Symposium on Radioactive Dating*, Vienna, Austria, November 19-23, 1962: 121-131.

Gray ST, Graumlich LJ, Betancourt JL et al. (2004) A tree-ring based reconstruction of the Atlantic Multidecadal Oscillation since 1567 AD. *Geophysical Research Letters* 31.

Grenander U (1959) *Probability and Statistics: The Harald Cramér Volume*. Alqvist & Wiksell, Stockholm.

Guyard H, Chapron E, St-Onge G et al. (2007) High-altitude varve records of abrupt environmental changes and mining activity over the last 4000 years in the Western French Alps (Lake Bramant, Grandes Rousses Massif). *Quaternary Science Reviews* 26: 2644-2660.

Hall VA and Pilcher JR (2002) Late-Quaternary Icelandic tephra in Ireland and Great Britain: detection, characterization and usefulness. *The Holocene* 12: 223-230.

Hansom J (2001) Coastal sensitivity to environmental change: a view from the beach. *CATENA* 42: 291-305.

Orme et al. (2015) *The Holocene*. DOI: 10.1177/0959683615596819

Heiri O, Lotter AF and Lemcke G (2001) Loss on ignition as a method for estimating organic and carbonate content in sediments: reproducibility and comparability of results. *Journal of Paleolimnology* 25: 101-110.

Higuchi K, Huang J, and Shabbar A (1999) A wavelet characterization of the North Atlantic oscillation variation and its relationship to the North Atlantic sea surface temperature. *International Journal of Climatology* 19: 1119-1129.

Hilton J, Lishman J and Allen P (1986) The dominant processes of sediment distribution and focusing in a small, eutrophic, monomictic lake. *Limnology and Oceanography* 31: 125-133.

Hurrell JW (1995) Decadal Trends in the North-Atlantic Oscillation - Regional Temperatures and Precipitation. *Science* 269: 676-679.

Hurrell JW and Van Loon H (1997) Decadal variations in climate associated with the north Atlantic oscillation. *Climatic Change* 36: 301-326.

Jones PD, Jonsson T and Wheeler D (1997) Extension to the North Atlantic Oscillation using early instrumental pressure observations from Gibraltar and south-west Iceland. *International Journal of Climatology* 17: 1433-1450.

Jordan JT, Smith DE, Dawson S et al. (2010) Holocene relative sea-level changes in Harris, Outer Hebrides, Scotland, UK. *Journal of Quaternary Science* 25: 115-134.

Kerr RA (2000) A North Atlantic climate pacemaker for the centuries. *Science* 288: 1984-1985.

Orme et al. (2015) *The Holocene*. DOI: 10.1177/0959683615596819

Kirk PL and Moberg EG (1933) Microdetermination of calcium in sea water.

*Industrial & Engineering Chemistry Analytical Edition* 5: 95-98.

Knudsen MF, Jacobsen BH, Riisager P et al. (2011) Evidence of Sues solar-cycle bursts in subtropical Holocene speleothem  $\delta^{18}\text{O}$  records. *The Holocene* 22: 597-602.

Kok JF, Parteli EJ, Michaels TI et al. (2012) The physics of wind-blown sand and dust. *Reports on Progress in Physics* 75: 106901.

Krantzberg G (1985) The influence of bioturbation on physical, chemical and biological parameters in aquatic environments: a review. *Environmental Pollution Series A, Ecological and Biological* 39: 99-122.

Kylander ME, Ampel L, Wohlfarth B and Veres D (2011) High-resolution X-ray fluorescence core scanning analysis of Les Echets (France) sedimentary sequence: new insights from chemical proxies. *Journal of Quaternary Science* 26: 109-117.

Kylander ME, Lind EM, Wastegård S et al. (2012) Recommendations for using XRF core scanning as a tool in tephrochronology. *The Holocene* 22: 371-375.

Lee G (1970) Factors affecting the transfer of materials between water and sediments. University of Wisconsin, Eutrophication Information Program, Literature Review No.1.

Leng M, Barker P, Greenwood P et al. (2001) Oxygen isotope analysis of diatom silica and authigenic calcite from Lake Pinarbasi, Turkey. *Journal of Paleolimnology* 25: 343-349.

Lomb NR (1976) Least-squares frequency analysis of unequally spaced data. *Astrophysics and space science* 39: 447-462.

Löwemark L, Chen HF, Yang TN et al. (2010) Normalizing XRF-scanner data: A cautionary note on the interpretation of high resolution records from organic-rich lakes. *Journal of Asian Earth Sciences* 40: 1250-1256.

Luterbacher J, Schmutz C, Gyalistras D et al. (1999) Reconstruction of monthly NAO and EU indices back to AD 1675. *Geophysical Research Letters* 26: 2745-2748.

Mackereth FJH (1969) Short core sampler for subaqueous deposits. *Limnology and Oceanography* 14: 145-151.

Marques R, Zêzere J, Trigo R et al. (2008) Rainfall patterns and critical values associated with landslides in Povoação County (São Miguel Island, Azores): relationships with the North Atlantic Oscillation. *Hydrological Processes* 22: 478-494.

Metcalf SE, Jones MD, Davies SJ et al. (2010) Climate variability over the last two millennia in the North American Monsoon region, recorded in laminated lake sediments from Laguna de Juanacatlán, Mexico. *The Holocene* 20: 1195-1206.

Met Office (2014 a) Stornoway climate averages (1981-2010). Available at:

<http://www.metoffice.gov.uk/public/weather/climate/gf77nswwt>

(Accessed 30/06/14)

Met Office (2014 b) Stornoway station data. Available at:

[http://www.metoffice.gov.uk/pub/data/weather/uk/climate/stationdata/stornoway\\_data.txt](http://www.metoffice.gov.uk/pub/data/weather/uk/climate/stationdata/stornoway_data.txt)

(Accessed 30/04/14).

Meyers PA (1994) Preservation of elemental and isotopic source identification of sedimentary organic matter. *Chemical Geology* 114: 289-302.

Moberg A, Sonechkin DM, Holmgren K et al. (2005) Highly variable Northern Hemisphere temperatures reconstructed from low-and high-resolution proxy data. *Nature* 433: 613-617.

Moisley H (1961) North Uist in 1799. *The Scottish Geographical Magazine* 77: 89-92.

Moreno A, Valero-Garcés B, González-Sampériz PI et al. (2008) Flood response to rainfall variability during the last 2000 years inferred from the Taravilla Lake record (Central Iberian Range, Spain). *Journal of Paleolimnology* 40: 943-961.

Olsen J, Anderson NJ and Knudsen MF (2012) Variability of the North Atlantic Oscillation over the past 5,200 years. *Nature Geoscience* 5: 808-812.

Pennington W, Tutin TG, Cambray RS et al. (1973) Observations on lake sediments using fallout  $^{137}\text{Cs}$  as a tracer. *Nature* 242: 324-326.

Pirazzoli P, Tomasin A and Ullmann A (2010) Recent changes in measured wind in the NE Atlantic and variability of correlation with NAO. *Annales Geophysicae* 28: 1923-1934.

Orme et al. (2015) *The Holocene*. DOI: 10.1177/0959683615596819

Press WH and Rybicki GB (1989) Fast algorithm for spectral analysis of unevenly sampled data. *The Astrophysical Journal* 338: 277-280.

Reimer PJ, Baillie MGL, Bard E et al. (2009) IntCal09 and Marine09 radiocarbon age calibration curves, 0-50,000 years cal BP. *Radiocarbon* 51: 1111-1150.

Reimer PJ, Bard E, Bayliss A et al. (2013) IntCal13 and Marine13 radiocarbon age calibration curves 0-50,000 years cal BP. *Radiocarbon* 55: 1869-1887.

Ritchie JC, McHenry JR and Gill AC (1973) Dating recent reservoir sediments. *Limnology and Oceanography* 18: 254-263.

Scargle JD (1982) Studies in astronomical time series analysis. II-Statistical aspects of spectral analysis of unevenly spaced data. *The Astrophysical Journal* 263: 835-853.

Serreze MC, Carse F, Barry RG et al. (1997) Icelandic low cyclone activity: Climatological features, linkages with the NAG, and relationships with recent changes in the Northern Hemisphere circulation. *Journal of Climate* 10: 453-464.

Shoelson B (2001) lombscargle.m. *MATLAB Central File Exchange*.

Available at:

<http://www.mathworks.co.uk/matlabcentral/fileexchange/993-lombscargle-m>

(accessed 30/4/14)

Silliman JE, Meyers PA and Bourbonniere RA (1996) Record of postglacial organic matter delivery and burial in sediments of Lake Ontario. *Organic Geochemistry* 24: 463-472.

Smith D and Fettes D (1979) The geological framework of the Outer Hebrides. *Proceedings of the Royal Society of Edinburgh. Section B. Biological Sciences* 77: 75-83.

Sorrel P, Debret M, Billeaud I et al. (2012) Persistent non-solar forcing of Holocene storm dynamics in coastal sedimentary archives. *Nature Geoscience* 5: 892-896.

Stabel H (1986) Calcite precipitation in Lake Constance: Chemical equilibrium sedimentation, and nucleation by algae. *Limnology and Oceanography* 31: 1081-1093.

Stephens WE and Calder A (2004) Analysis of non-organic elements in plant foliage using polarised X-ray fluorescence spectrometry. *Analytica chimica acta* 527: 89-96.

Telford R, Heegaard E and Birks H (2004) All age-depth models are wrong: but how badly? *Quaternary Science Reviews* 23: 1-5.

Trouet V, Esper J, Graham NE et al. (2009) Persistent Positive North Atlantic Oscillation Mode Dominated the Medieval Climate Anomaly. *Science* 324: 78-80.

Trouet V, Scourse JD and Raible CC (2012) North Atlantic storminess and Atlantic Meridional Overturning Circulation during the last Millennium:

Reconciling contradictory proxy records of NAO variability. *Global and Planetary Change* 84-85: 48-55.

Van Loon H and Rogers JC (1978) The Seesaw in Winter Temperatures between Greenland and Northern Europe. Part I: General Description. *Monthly Weather Review* 106: 296-310.

Wanner H, Brönnimann S, Casty C et al. (2001) North Atlantic Oscillation - Concepts and Studies. *Surveys in Geophysics* 22: 321-381.

Weaver BL and Tarney J (1981) Lewisian gneiss geochemistry and Archaean crustal development models. *Earth and Planetary Science Letters* 55: 171-180.

Weltje GJ and Tjallingii R (2008) Calibration of XRF core scanners for quantitative geochemical logging of sediment cores: Theory and application. *Earth and Planetary Science Letters* 274: 423-438.

White DS and Miller MF (2008) Benthic invertebrate activity in lakes: linking present and historical bioturbation patterns. *Aquatic Biology* 2: 269-277.

Yancheva G, Nowaczyk NR, Mingram J et al. (2007) Influence of the intertropical convergence zone on the East Asian monsoon. *Nature* 445: 74-77.

Yang D and Myers PG (2007) Impact of extended NAO buoyancy forcing on the subpolar North Atlantic and climate variability over the last millenium. *Paleoceanography* 22: PA3104.